Loss of the Low-Frequency Component of the Global-Flash Multifocal Electroretinogram in Primate Eyes with Experimental Glaucoma

Xunda Luo, Nimesh B. Patel, Ronald S. Harwerth, and Laura J. Frishman

Purpose. To study relationships between glaucoma-sensitive components identified with frequency-domain analysis of global-flash multifocal electroretinogram (mfERG), regional retinal nerve fiber layer thickness (RNFLT), and local visual field sensitivity (VS).

Methods. Eleven macaque monkeys, including four controls and seven with unilateral laser-induced trabecular meshwork scarification and ocular hypertension, were observed with optical coherence tomography (OCT), full-field light-adapted flash ERG, 103-hexagon global-flash mfERG (MFOFO), and static perimetry. The effects of experimental glaucoma on mfERG were assessed in the frequency domain. Relations between root mean square (RMS) amplitude of a glaucoma-sensitive frequency range and peripapillary RNFLT (standard 12° OCT circular scan), and between RMS amplitude and VS were studied.

Results. Experimental glaucoma led to a dramatic and consistent power loss in the low-frequency (<25 Hz) band of mfERG. The RMS of this low-frequency component (LFC) correlated significantly with the regional RNFLT. The r^2 of linear fits was 0.39 ($P < 0.001$) for cross-sectional group data and 0.60 after correction for intersubject variability. The r^2 of linear fits for longitudinal data from individual animals was as high as 0.78 ($P < 0.001$). Local LFC RMS amplitude also correlated significantly with interpolated VS for hexagons. The r^2 for exponential fits of hexagon LFC RMS amplitudes (inner three rings) versus VS (dB) was 0.29 to 0.52 ($P < 0.001$) for the group and up to 0.95 in individuals.

Conclusions. The significant correlations between regional measures of global-flash mfERG, RNFLT, and VS suggest that LFC RMS amplitude provides a useful index for objective quantification of local RGC function and monitoring of early changes in glaucoma. (*Invest Ophthalmol Vis Sci.* 2011;52:3792–3804) DOI:10.1167/iovs.10-6667

The multifocal (mf)ERG technique, developed by Sutter and Tran,[1] is a noninvasive method for simultaneous functional testing of multiple retinal locations. The stimuli are presented in a pseudorandom m-sequence. A fast-flicker mfERG protocol (typically, 75 Hz) with $2^{14} - 1$ m-steps can test more than 100 retinal regions in less than 7 minutes of recording time, providing sufficient spatial resolution and signal-to-noise ratio (SNR) to resolve focal defects with clinically acceptable time efficiency.

Although the mfERG technique has been demonstrated to be useful in the diagnosis and monitoring degenerative diseases of the outer retina as well as some diseases that affect inner retina (such as diabetic retinopathy[2,3]), its value in diagnosis and monitoring of progression of glaucoma, a disease that mainly affects retinal ganglion cells (RGCs) and their axons, remains controversial. It has been noted that the nasotemporal asymmetry in mfERG waveforms in the fast flicker mfERG is reduced or eliminated by both tetrodotoxin (TTX, a blocker of sodium-dependent action potentials) injected intravitreally (in monkeys) and glaucoma (in monkeys and humans), indicating an inner retinal origin, mainly RGCs, of this phenomenon.[4–8] Effects of TTX and experimental glaucoma on nasotemporal asymmetry have also been described in monkeys for the slow-sequence mfERG, in which the flicker rate was slowed by interposing 7 to 14 black frames between each m-step.[9–11]

The nasotemporal asymmetry can be accounted for by the optic nerve head component (ONHC) model proposed by Sutter and Bearse,[12] which links the asymmetry mainly to the different regional delays in propagation of action potentials in the unmyelinated RGC axons carrying these signals to the optic nerve head (ONH). Action potentials traveling a longer distance (e.g., from temporal retina) before arriving at the ONH are relatively delayed compared with those traveling a shorter distance (e.g., from the nasal retina). The mfERG component reflecting these delays is identified in the model of Sutter and Bearse as the ONHC, whereas the component devoid of these delays is called the retinal component (RC). The ONHC can be extracted from control mfERG recordings in both humans and monkeys with a time-domain algorithm introduced by Sutter and Bearse.[12,13]

The ONHC can be enhanced in the first-order kernel signal of the mfERG by appending one or more global flashes after the m-frame.[14,15] Waveforms obtained with these global flash paradigms are usually divided into a direct component (DC) and one to several induced component(s) (IC) for analysis. The DC is the direct response to the focal flash, whereas the IC is the response to the corresponding global flash under the influence of the preceding focal flash, a response that is believed to be generated in the inner retina.[16,17] Several global-flash paradigms have been used, DC and ICs have been measured, and the ONHC has been extracted with the algorithm to assess inner retinal function.[9,10,12,13,16,18–20]

The validity of the relation between the ONHC and inner retina function has been based on studies of glaucoma, which is a disease of RGC loss in the inner retina. Consequently, the ONHC should also be correlated with other clinical measures of RGC function, such as visual field sensitivity (VS) and peri-

From the College of Optometry, University of Houston, Houston, Texas.

Supported by National Eye Institute Grants R01-EY06671 (LJF), R01-EY01139 (RSH), and P30-EY07751 (University of Houston College of Optometry).

Submitted for publication October 2, 2010; revised February 9, 2011; accepted March 2, 2011.

Disclosure: **X. Luo**, None; **N.B. Patel**, None; **R.S. Harwerth**, None; **L.J. Frishman**, None

Corresponding author: Laura J. Frishman, College of Optometry, University of Houston, 505 J. Davis Armistead, Houston, TX 77204-2020; lfrishman@optometry.uh.edu.

papillary retinal nerve fiber layer thickness (RNFLT). The relationship between the ONHC and RNFLT is especially interesting, because it does not involve a psychophysiological link and, in fact, may represent two objective measures of the stage of neuropathy. However, the nature of the relationships between the mfERG ONHC, regional peripapillary RNFLT, and local VS have not been studied quantitatively. The purpose of the present study was to investigate this issue in a frequency-domain approach that has shown promise in several recent studies for identifying focal changes in frequency bands of mfERG responses that include contributions from the ONHC.[10,11,21] Some of the findings have been reported previously in abstract form (Luo X, et al. *IOVS* 2007;48:ARVO E-Abstract 5982).

METHODS

Subjects

Eleven adult rhesus monkeys (*Macaca mulatta*, 7–8 years old, of both sexes) were included in the study. Four monkeys were normal subjects. As a model of experimental glaucoma, seven others underwent unilateral laser scarification of the trabecular meshwork (TM) while under general anesthesia, to induce ocular hypertension,.[22,23] All experimental and animal care procedures adhered to the ARVO Statement for the Use of Animals in Ophthalmic and Vision Research and were reviewed and approved by the Institutional Animal Care and Use Committee of the University of Houston.

Animal Preparation

The animals were anesthetized intramuscularly with ketamine (20–25 mg/kg/h) and xylazine (0.8–0.9 mg/kg/h) and were treated with atropine sulfate (0.04 mg/kg injected SC), as previously described.[11,21] Body temperature was maintained between 36.5°C and 38°C with a thermostatically controlled blanket (TC1000 temperature controller; CWE, Ardmore, PA). Heart rate and blood oxygen were monitored with a pulse oximeter (model 44021; Heska Corp., Des Moines, IA). Pupils were fully dilated to approximately 8.5 mm in diameter with topical tropicamide (1%) and phenylephrine (2.5%). In the mfERG experiments, the monkey eyes were refracted and fitted with contact lenses appropriate for the viewing distance, and the foveas were centered to the stimulus midpoint with a modified direct ophthalmoscope (American Optical Co., Buffalo, NY). For OCT experiments, a plano-power contact lens was fitted on the eye to maintain optical clarity. A bite bar and an occipital bar attached to a rotational mount were used to adjust the position and stabilize the head of the animal.[24]

ERG Experiments

Previous studies have indicated that the function of the outer retina as measured by a- and b-wave amplitude in photopic, brief, full-field flash ERG does not change in glaucoma, whereas the function of the inner retina, as measured by photopic negative response (PhNR, a slow negative component after the b-wave), is very sensitive to glaucoma in human subjects and the primate model used in the present experiments.[25–28] In this study, brief full-field photopic flash ERGs were recorded (DC, 1000 Hz; Espion system; Diagnosys, Lowell, MA), to assess both outer and inner retinal function. The stimuli were brief red flashes (λ_{max} = 650 nm, 0.04–2.84 cd s/m^2) on a rod-saturating blue background (λ_{max} = 462 nm, 10 cd/m^2, 100 scotopic cd/m^2) and brief white flashes (0.04–22.72 cd s/m^2) on a white background (40 cd/m^2, 100 scotopic cd/m^2). The red flashes on blue background were used to optimize PhNR recordings,[26] and the white stimuli, for comparison with the mfERG recordings of pre–ganglion cell contributions to the ERG for a stimulus of wavelength similar to that used for the mfERG. A 103-element, unstretched hexagon array (VERIS [Visual Evoked Response Imaging System 4.1]; Electro-Diagnostic Imaging, Inc., Redwood City, CA) was used for mfERG recording. The hexagon array subtended an angle of approximately 35° × 34° on the retina at a viewing distance of 46 cm (Fig. 1A). The ONH in the monkeys was approximately 16.5° from the fovea, on the nasal edge of the retinal projection of the hexagon array (Fig. 1B). The frame rate of the CRT stimulus monitor was 75 Hz. As in the ONHC MFOFO VERIS 5 protocol, our protocol had five frames in each m-step. The first frame contained focal flashes (2.7 cd s/m^2) controlled by the VERIS pseudorandom m-sequence. The second and fourth frames contained global flashes (2.7 cd s/m^2), and the third and fifth frames were dark (~0.2 cd s/m^2 with the room lights on).

This resulting stimulus was different from the VERIS 5 protocol in two respects. First, the surround of our stimulus was dark (15 cd/m^2)

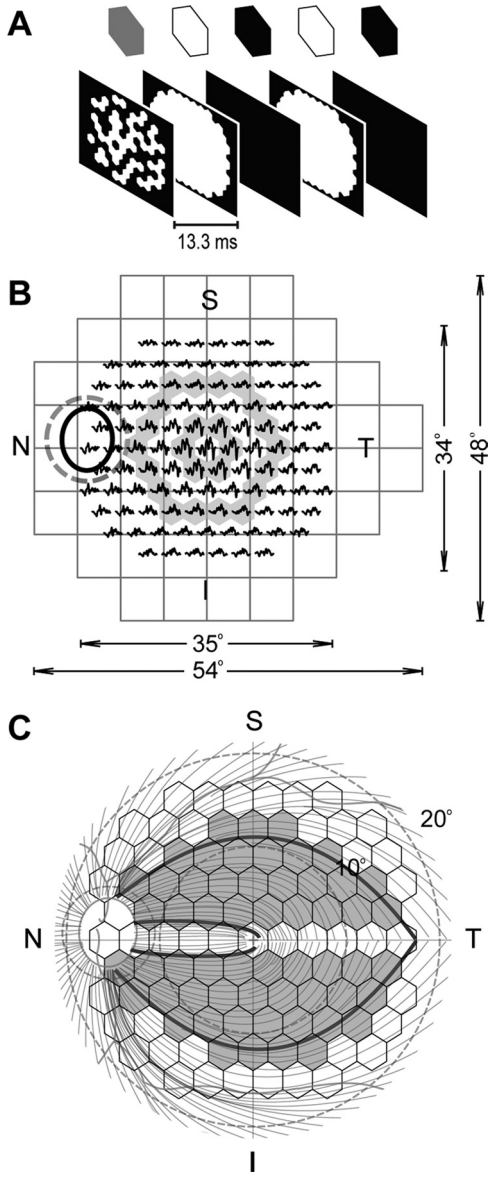

FIGURE 1. (**A**) The two-global-flash paradigm used in this study. (**B**) Testing area of a 24-2 standard automated perimeter and the 103-element array used for mfERG shown for the left eye with retinal orientation. *Ellipse*: the ONH: *dashed circle* around the ONH: a standard 12° OCT circular scan. *Shaded area*: rings 1 and 3. Central hexagons show larger response amplitudes, while nasotemporal asymmetry is easier to identify in larger rings. (**C**) The axon course map based on Shields,[32] used for analysis of conduction velocity illustrated in Figure 5 and indicating, for the correlation analysis illustrated in Figure 7, the hexagons and peripapillary arcs (portions of the *dashed circle* defined by the axons projecting from the highlighted hexagons) that were used.

rather than equal to the mean luminance of 55 cd/m^2 of the hexagon array. Since the array covered almost the entire CRT screen, with room lights on during stimulation and calibration and appropriate preadaptation to light, the narrow surround would have had little effect on a subject's adaptation status. Second, the hexagon array was not stretched due to differences in macaque versus human eyes, for which stretch parameters are provided in VERIS 5.

The animals were maintained under general anesthesia during mfERG recordings in a regimen that minimized eye movements.[29] With these relatively stable recording conditions, compared with those encountered in conscious humans, no artifact-rejection algorithm was used, even though the amplifier filter setting extended to low frequencies (i.e., 1–300 Hz; model 5A22N; Tektronix, Beaverton, OR), as in previous studies of macaques from the laboratory. Two 9-minute recordings were collected and combined in VERIS for each eye. First-order kernel responses (0–250 ms) were derived, and, because data collected with the chosen parameters were rather noisy, the derived kernels were averaged (three iterations, 17%) to improve the SNR before data were exported for offline analysis.

In this article, all figures showing hexagon arrays are oriented to display the retinal view.

ERG Signal Offline Processing

Photopic full-field, brief-flash ERG recordings were filtered with a DC 80-Hz digital filter. A potential surrogate for RGC function was assessed by measuring the amplitude of the PhNR from baseline, 65 ms after the onset of a 2.84-cd s/m^2 flash.[11] This measurement was reversed in sign so that the PhNR amplitude had a positive sign in normal recordings and decreased, often to a negative number on the other side of the baseline in eyes with experimental glaucoma. A-wave amplitude was measured from the baseline to the trough and b-wave amplitude, from the trough of the a-wave to the peak of the b-wave.

Fast Fourier transform (FFT) of the averaged mfERG response for the entire trace array was multiplied with its complex conjugate to calculate the power spectra (MatLab ver. 7.01; The MathWorks, Inc., Natick, MA). A glaucoma-sensitive frequency band was identified by comparing the power spectra from control and fellow eyes with experimental glaucoma and was used as a reference in designing a digital filter with linear phase spectra. This filter was used to isolate glaucoma-sensitive components from original mfERG recordings for further analyses.

The ONHC (and RC) in control recordings was extracted with a time-domain algorithm based on Sutter and Bearse,[12] using the following approach. Since the implicit time of the ONHC varies relative to that of the RC across the retina, averaging focal responses time locked to the ONHC by shifting the traces according to landmarks of nasotemporal asymmetry smears the RC and preserve the ONHC in the averaged response. In contrast, averaging focal responses time locked to the RC (i.e., with no or little shift of the traces) smears the ONHC in the time domain, leaving an approximation of the RC in the averaged response. Successive approximations of the ONHC and RC continued until the stop criterion was met, when 95% of the energy of the original signals could be represented by the isolated ONHC and RC. It typically took 50 to 100 iterations to meet the criterion.

The algorithm was used to extract the ONHCs from third-ring-hexagon responses (Fig. 1B). The choice of ring 3 was made to balance two competing factors that affect performance of the algorithm. On the one hand, cone-mediated mfERG response density and RGC density and hence mfERG response amplitudes decrease with eccentricity. For this somewhat limiting reason, it would be best to use signals from the most central ring for ONHC extraction. On the other hand, averaging responses from a larger ring with more hexagons should improve signal-to-noise (SNR). Another advantage of using a larger ring is that the nasotemporal asymmetry is easier to identify. For this reason, ring 3, which has 18 hexagons, was chosen for ONHC extraction.

Perimetry and Data Interpolation

As part of other concurrent studies, static perimetry was performed frequently on five of the animals with experimental glaucoma (Humphrey Field Analyzer; [HFA] model 630; Carl Zeiss Meditec, Dublin, CA), with the central 24-2 full-threshold program and a Goldmann size III target (0.43° in diameter). Details have been provided previously.[30]

Compared with the mfERG hexagon array, a standard 24-2 HFA program tests fewer locations over a larger area of the retina (Fig. 1B). We compared local mfERG and VS by bilinearly interpolating VS results, a procedure demonstrated to be comparable in accuracy to using a modified Humphrey field, in which the perimetry test spots were centrally placed in the hexagons.[8,31] Global and local visual sensitivities, rather than mean deviation (MD) and total deviation, were used for data analysis and results, as these values give a direct measure of function.

Optical Coherence Tomography

All the OCT RNFLT scans were acquired by one operator (NBP) with the Stratus OCT (software version 4.0.4; Carl Zeiss Meditec) on three subjects (OHT-51, -48, and -53) and later with the Spectralis HRA+OCT (Heidelberg Engineering, Heidelberg, Germany) on four subjects (OHT-57, -59, -60, and -61). The standard 12° RNFLT protocol was used without modification. Three 512-point (Stratus) or 1536-point (Spectralis) scans were obtained for each eye and exported for further analysis.

As part of our other studies, the agreement between the Stratus and Spectralis OCTs on peripapillary RNFLT measurements was examined in 20 normal monkey eyes on which both instruments were used on the same day. RNFLTs measured with Spectralis were thicker than those measured with Stratus (our unpublished observations, 2008–2009). The relation between the two measurements was found to be linear (Stratus RNFLT = 0.87 × Spectralis RNFLT + 5.6). This observation allowed us to convert Spectralis data into Stratus equivalents and pool all OCT data for further analysis.

Axon Course Map

The empiric axon course map used in this study (Fig. 1C) was a digitized image of the map provided by Shields,[32] originally based on data from monkey eyes[33–36] and adjusted for humans. To date, a course map specifically constructed for macaques is not, to our knowledge, available. The course map was used to estimate the projections of hexagons on the standard 12° OCT circular scans to study the relation between peripapillary RNFLT and mfERG functional measures for the hexagons.

Ultrasound

The axial lengths of seven normal eyes in the macaques were measured by one examiner (3D/B/A-Scan Ophthalmic Ultrasound Scan1000; OTI Ophthalmic Technologies Inc., Toronto, ONT, Canada). Ten high-quality measurements were acquired for each eye and averaged to obtain the axial length. These measurements were used in calculations of retinal axon length.

Data analyses, aside from those that have already been described, will appear in relevant sections of the Results.

Results

Relations between Global Measures of RNFLT, VS, and PhNR Amplitude in Experimental Glaucoma

Structural (OCT) and functional (perimetry, full-field flash ERG and mfERG) examinations were performed on the animals at different stages of experimental glaucoma. Of the seven animals that received TM lasering, all were tested with OCT, full-field flash ERG, and mfERG, and all but two were also evaluated with perimetry. Global structural and functional measurements for all the animals around the time of each ERG/mfERG recording session are listed in Table 1.

As observed in previous studies, neither a- nor b-wave amplitudes in full-field flash ERGs were reduced in eyes with

TABLE 1. Global Measures for Functional and Structural Tests in Control and Fellow Eyes with Experimental Glaucoma

		Average RNFL Thickness (μm)		HFA Sensitivity (dB)		R/B PhNR Amplitude (μV)		LFC Power ($\times 10^7$ nV^2Hz^{-1})	
Animal		**Con**	**Exp**	**Con**	**Exp**	**Con**	**Exp**	**Con**	**Exp**
OHT-51	1	86.1	40.4	31.4	28.4	42.4	0.8	20.2	4.7
OHT-48	1	94.5	46.4	33.5	26.0	32.3	−18.8	25.9	4.3
OHT-57	1	99.6	91.2	30.4	29.9	31.0	21.3	14.3	7.2
	2	101.0	88.5	30.1	29.4	36.2	10.5	11.5	4.5
OHT-59	1	97.6	100.3			26.1	16.6	10.6	8.9
	2	98.7	90.1				6.1	7.7	7.6
	3	100.5	83.8			15.9	0.7	9.1	5.7
OHT-60	1	99.4	96.6			64.1	82.7	16.0	21.6
	2	96.3	91.6	30.9	31.7	76.5	39.4	11.6	7.0
	3	94.7	72.4	30.3	32.0	76.3	26.2	11.6	6.7
	4	94.8	68.9	30.7	28.1	79.5	18.3	9.9	2.5
OHT-61	1	103.7	57.2			16.7	−29.9	34.6	5.8
OHT-53	1	101.5	95.0	32.8	28.5	26.7	−1.8	33.3	11.7
	2	99.3	83.2	32.9	28.0	19.6	−12.5	27.0	8.6
	3	101.5	66.4	31.8	27.3		−25.4	24.7	3.9
	4	97.6	65.6	33.3	27.1	24.9		31.2	4.9
	5	95.6	55.5	33.2	24.9	18.7	−18.6	28.2	6.0
	6	98.2	58.6	33.5	22.7	13.3	−24.2	18.3	5.1

Global measures for structural (OCT) and functional (perimetry, full-field red flash ERG and mfERG) tests performed on each animal with unilateral experimental glaucoma in the study. Con, control eye; Exp, fellow eye with experimental glaucoma.

experimental glaucoma. Generally, no changes have been reported, but in the present study, a-wave amplitudes, measured on the leading edge, were slightly increased in response to both red and white test stimuli (Table 2). In contrast, the PhNR amplitude declined as peripapillary RNFLT and VS, averaged for the whole field, declined in eyes with experimental glaucoma. Figure 2 shows that for PhNR amplitude, RNFLT, and VS, declining values seen in eyes with experimental glaucoma (Exp, filled circles) showed a continuum with data from control eyes (Con, open circles), allowing data from both eyes to be fit adequately with one function. This observation is consistent with the assumption that these measures are all related to the number of RGCs, which declines with disease progression. The correlations among these functional and structural measures were all statistically significant, whether the analysis was based on a longitudinal dataset from an individual animal (OHT-53, top row) collected over a course of 15 months (the longest follow-up period in the study; Table 1) as neuropathy in this animal progressed (Figs. 2A–C) or on a cross-sectional dataset that included only the last session from each of the seven animals with experimental glaucoma (Figs. 2D–F, main panels). The complete dataset from all sessions for all seven animals are plotted in the insets of Figures 2D–F to show the similarity of the overall distribution to the longitudinal (Figs. 2A–C) or cross-sectional data (Fig. 2D–F).

Previous studies have shown that RNFLT and global and focal ERG functional measures asymptote to their residual levels or exceed their dynamic ranges, when MD is worse than −10 to −15 dB.[37–39] We may not have been able to see this phenomenon in our data because of the limited loss of VS in our animals. The largest interocular difference in VS recorded from our animals was 10.7 dB.

Losses of Nasotemporal Asymmetry and LFC Power Occurred in mfERG Signals from Eyes with Experimental Glaucoma

As in previous reports, nasotemporal asymmetry in mfERG responses was disrupted by experimental glaucoma. Figure 3A shows trace arrays from both eyes of OHT-48 with third-ring responses highlighted. Loss of nasotemporal asymmetry is easier to identify when these responses are stacked (Fig. 3B, showing six traces from corner hexagons of the third ring) for the Con (OS, left) and Exp (OD, right) eye. Asymmetry for the

TABLE 2. Effects of Experimental Glaucoma on a- and b-Waves in Full-Field Flash ERGs Elicited with White Flashes on White Backgrounds (W/W) and Red Flashes on Blue Backgrounds (R/B)

	All Animals, All Sessions Tested (n = 14)				All Animals, Last Session (n = 7)			
	Con	**Exp**	t	P	**Con**	**Exp**	t	P
W/W								
a-Wave @ 6 ms	−13.1 ± 6.2	−16.4 ± 5.3	3.43	0.004	−12.3 ± 6.4	−16.6 ± 7.2	3.53	0.012
b-Wave @ 30 ms	95.5 ± 36.2	93.6 ± 36.5	0.29	0.777	93.6 ± 24.8	82.5 ± 30.6	1.93	0.101
R/B								
a-Wave @ 6 ms	−11.2 ± 2.8	−14.4 ± 3.2	3.88	0.002	−10.8 ± 2.5	−14.7 ± 4.6	3.13	0.020
b-Wave @ 30 ms	97.2 ± 31.6	96.0 ± 36.2	0.29	0.780	98.8 ± 25.4	91.4 ± 34.6	1.91	0.105

Data are expressed as amplitude in microvolts ± SEM. Only the responses to the highest stimulus energy, 2.84 cd · s/m^2, were measured. Flash ERGs were not recorded in four sessions; hence, n = 14, rather than 18 for all sessions.

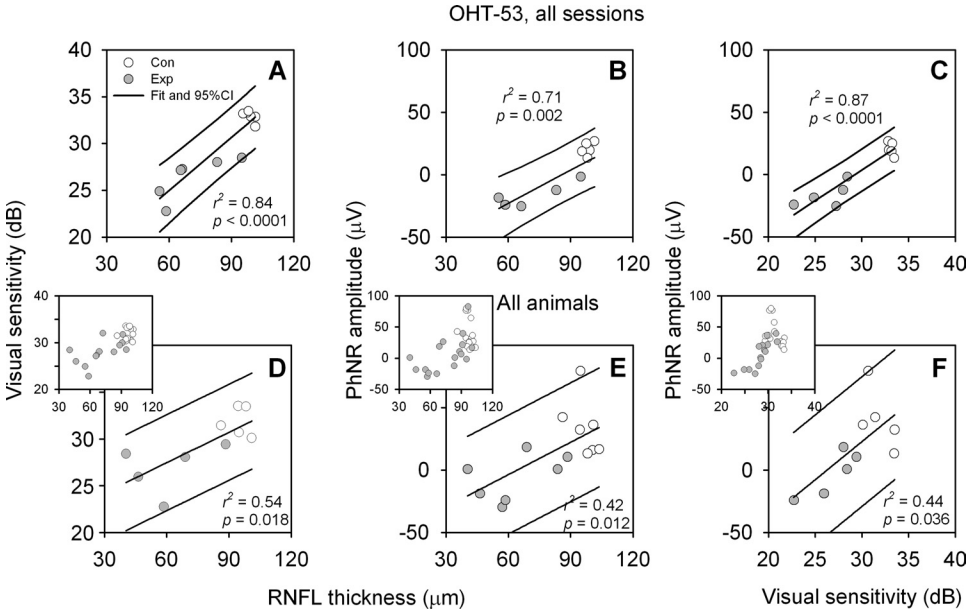

FIGURE 2. Relations between average RNFLT, VS, and PhNR amplitudes (measured for the response to a flash of 2.84 cd · s/m^2). (**A–C**) Data from multiple imaging and recording sessions for subject OHT-53 only; (**D–F**) data from the last session of each animal (*main panels*) and all sessions of all animals (*insets*). *Open circles*: data from control (Con) eyes; *gray circles*: data from fellow Exp eyes. *Solid lines*: linear fits and 95% PI for data from both eyes. There were only five PhNR recordings available for each eye of subject OHT-53, as indicated in Table 1.

Con eye is best seen when the most nasal (N) and most temporal (T) traces are compared. The nasotemporal asymmetry seen in the control recordings reflects the asymmetry seen in the extracted ONHC for each record. For instance, the circles placed on the control recordings (Fig. 3B, left column, black traces) mark a trough that shows implicit time shifts with location. This trough is very close to N2 in the ONHCs extracted from these control recordings (Fig. 3B, left, gray traces). However, the extracted ONHCs lacked some small high-frequency oscillatory features that can be easily seen in the Con eye records, many of which were eliminated by glaucoma.

Certain high-frequency features were more obvious in the extracted RC (Fig. 3B right column, gray traces), especially late in the RC between 50 and 70 ms where they rested on top of a prominent slow response. Residual responses of the Exp eye showed little nasotemporal asymmetry or changes in implicit time with distance from the ONH (right column, black traces). Although these residual responses resembled corresponding RC responses from the control recordings, the late high-frequency activity noted above was lost or reduced in glaucoma. This observation suggests that the RCs were also changed, to some extent by glaucoma. The loss of more high-frequency, oscillatory activity in the Exp eye than was present in either the extracted ONHC or the RC also indicates that some of that activity in the Con eye records was formed by additive interactions of signals that occurred in different phases in the ONHC and RC, as previously proposed.[9,11,21,40,41]

In addition to the oscillatory activity, a prominent slower response that appeared in the control records was reduced or eliminated by glaucoma. Depending on hexagon location, the affected responses started at 10 to 20 ms or later in control records in Figure 3B (and in surface plots of the same data in Fig. 4B) and they were largest between approximately 30 and 70 ms. In addition to including characteristics of the ONHC, these responses included contributions from the DC and ICs that have been analyzed by other investigators in global-flash mfERG studies.[17,18] However, in the present study, the DC and ICs could not be separately quantified. They were overlapped because of the specific global flash paradigm, MFOFO (Fig. 1A), that was used. The video frame for the first global flash of the MFOFO followed immediately after the m-frame (i.e., at 13.3 ms), whereas for the MOFO paradigm used by other investigators, a black frame occurred between the m-frame and global flash,[17,18] which allowed more separation of IC1 in time from the earlier DC response. We used a second global flash late in the paradigm (53.2 ms) as well, but there was not much IC2 visible late in the record, after 70 ms.

The nasotemporal asymmetries in various peaks and troughs of the control records in Figures 3B and 4B occurred both early in the record when the DC was starting and later in the response when the DC and ICs overlapped. These asymmetries were all eliminated by experimental glaucoma (Figs. 3B, 4C) regardless of time in the record. This result suggests that the asymmetry, which is the defining feature for the ONHC, is present in both the DC and ICs, and further, that these two ways to analyze mfERG signals (into ONHC and RC versus into DC and IC) are not mutually exclusive.

A further complication in quantifying effects of experimental glaucoma on global-flash mfERG was the problem encountered in isolation of ONHC and RC in glaucomatous eyes. The reduction or elimination of nasotemporal asymmetry made it difficult to apply the algorithm to extract ONHC and RC, as application of the algorithm was based, for our small subject group, on the use of identifiable nasotemporal asymmetry in individual eyes. Due to these problems with previously applied analyses, we tried a different approach, which was to look at glaucomatous changes from the perspective of the portions of the temporal frequency domain that might be affected.

Figure 4A shows typical power spectra of the mfERG averaged over the hexagon array for an individual subject (OHT-48, same subject as in Fig. 3) on the left and for the group of all seven animals with unilateral experimental glaucoma on the right. To obtain the power spectra for the group, individual amplitude spectra from one session from each animal were first averaged and then squared. In control eye recordings, a significant portion of signal power came from a low-frequency band with a turning point at 24.6 Hz. This low-frequency signal peaked at 12.1 Hz (SD 1.1) and decayed to half amplitude at 18.3 Hz (SD 1.6). When comparing power spectra from fellow eyes with experimental glaucoma (confirmed by loss of VS, or average RNFLT, or both) to those of Con eyes, we identified a dramatic and consistent power loss in this large, low-frequency signal.

Based on the finding in the power spectra, a low-pass digital filter with a cutoff frequency of 25 Hz and a linear phase spectra was designed to isolate the low-frequency signal from mfERG recordings. In the 3-D color-coded surface plots in

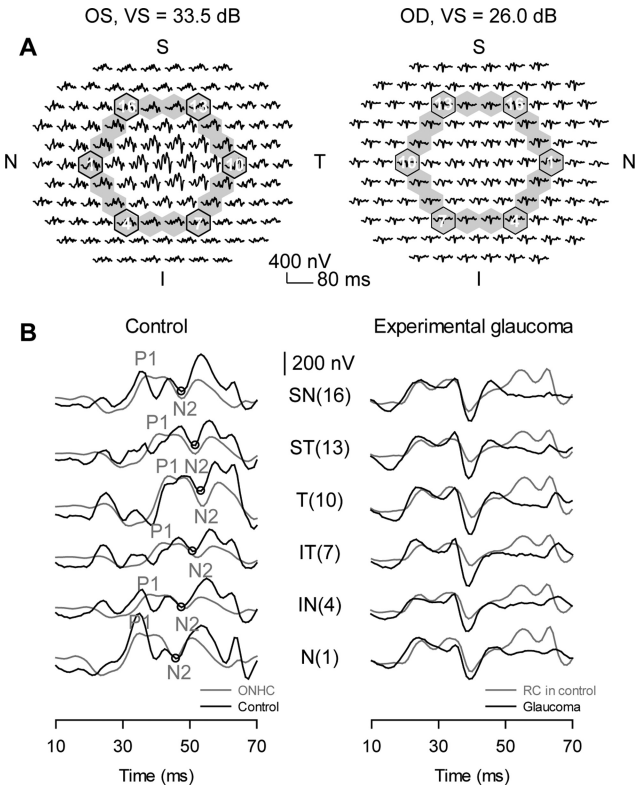

FIGURE 3. Loss of nasotemporal asymmetry in experimental glaucoma. (**A**) Trace arrays from the Con and Exp eyes of subject OHT-48 with third-ring responses highlighted, and six-corner hexagons marked on the trace array. (**B**) *Left*: traces from six-corner hexagons of the third ring of the Con eye (OD); *right*: and the Exp eye (OS; *black traces*). The systematic change in implicit time of a negative component is highlighted in the Con eye recordings (*left*) with an *open circle* and a *gray* line. The *gray traces* in the *left* column represent extracted ONHCs from the same Con eye recordings. The *gray traces* in the right column represent RCs from the Con eye recordings in the left column. The numbers in parentheses show the corresponding hexagon numbers for the third-ring traces. P1 and N2: the first peak and second trough in the ONHC; SN, superonasal; ST, superotemporal; T, temporal; IT: inferotemporal; IN, inferonasal; N, nasal.

Figures 4B and 4C, nasotemporal asymmetry can be easily identified in Con eye recordings (Fig. 4B), but not in recordings from the Exp eye (Fig. 4C). Nasotemporal asymmetry was also present in the isolated low-frequency component (to be termed the LFC) of the Con eye recording, shown in Figure 4D. Almost all the LFC, including any asymmetry, was missing from the Exp eye records (Fig. 4E). As seen for the ONHC extracted with the algorithm based on nasotemporal asymmetry (Fig. 3B), the LFC extracted with the low-pass filter in Figure 4D also spanned the time window for DC and overlapped DC and ICs, making it potentially useful as an inclusive measure for assessing glaucomatous changes in the MFOFO global-flash mfERG.

The MFOFO paradigm was not optimal for generating the high-frequency OPs (e.g., 110–224 Hz) that were seen to be sensitive to glaucoma or optic atrophy in previous studies using slow-sequence mfERG protocols.[9,11,21,42] Although the loss of high-frequency components was obvious, as noted above, the power of the components, and changes seen in the power spectra were small (insets to plots in Fig. 4A) compared to power and loss of LFC. For these reasons, all subsequent analyses in the frequency domain were focused on the LFC.

Axon Conduction Velocity Estimated with the ONHC and LFC

Since the LFC demonstrated nasotemporal asymmetry and this asymmetry was reduced in eyes with experimental glaucoma (as documented by loss of RNFLT and worsening of VS), we hypothesized that LFC reflects function of RGCs and their axons, and receives contributions from the same mechanisms that generate the ONHC. We used the following experiment to test this hypothesis, by seeing how well the implicit time information of the ONHC is preserved in the LFC.

The ONHC was extracted from the original recordings with the algorithm, and the LFC was isolated from the original recordings with the low-pass filter from seven normal eyes, including the three control eyes of OHT-51, -48, and -53 and four eyes from four control animals. Axonal conduction velocity for the third ring of the mfERG stimulus was estimated from the P1 (Fig. 3B, left column) implicit time change of the ONHC (Fig. 5A) and from the time shift of the LFC determined with cross-correlation (Fig. 5B, referenced to trace from hexagon 18, which is just superotemporal to hexagon 1). Distances from the centers of hexagons in the third ring, to the ONH, along axon trajectories, were estimated based on Shields' map[32] (Fig. 1C) and a modified four-surface schematic eye of macaque monkey proposed by Lapuerta and Schein.[43] For each eye, axonal conduction velocity was calculated by relating time delays and distances from the ONH (Fig. 5). The conduction velocities estimated with the two methods were 0.82 ± 0.07 m/s (mean ± SD for the seven eyes) and 0.97 ± 0.22 m/s, respectively. The difference between these two measures was not statistically significant (paired 2-tailed *t*-test, $t = 0.99$; $P = 0.36$), and both were within the range of conduction velocities estimated and measured directly in humans and monkeys (0.4–1.2 m/s).[12,13,44–47] This finding supports the hypothesis that the ONHC and the LFC share a common generating element, presumably, unmyelinated ganglion cell axons.

Relation between LFC RMS Amplitude, Average RFNLT, VS, and PhNR Amplitude in Full-Field, Red-Flash ERG

To compare the LFC with the other global structural and functional measures of RGCs, we first quantified LFC in terms of RMS amplitude calculated from the average mfERG trace in the signal window from 10 to 70 ms, which corresponded to the window that showed maximum nasotemporal asymmetry (and covered time windows including both DC and overlapping IC1). Figure 6 shows distributions of global LFC, RNFLT, VS, and PhNR data for all sessions of one animal (Figs. 6A–C) and the last session only for each animal (Figs. 6D–F). The insets show data from all sessions of all animals. Compared with the other three measures, a dramatic decrease in global LFC RMS amplitude could be seen even in the early stage of the disease, and there was not much overlap between Con and Exp data. These observations are consistent for all three datasets plotted in Figure 6.

Linear regression analyses were performed for Exp eye data only in Figure 6: between RMS amplitude and average RNFLT (Fig. 6A and main panel in 6D), between RMS amplitude and average VS (Figs. 6B, 6E), and between RMS amplitude and PhNR amplitude (Figs. 6C, 6F). The correlations between these global measures were better defined in OHT-53, with the strongest between the LFC and the PhNR ($r^2 = 0.84$, $P = 0.010$; Fig. 6C). The correlations deteriorated when interindividual variability was introduced (Figs. 6D–F).

For these global measures, it is important to note that the hexagon array covered only the central retina, from fovea to approximately 17.5° eccentricity. RNFLT plotted in Figure 6A

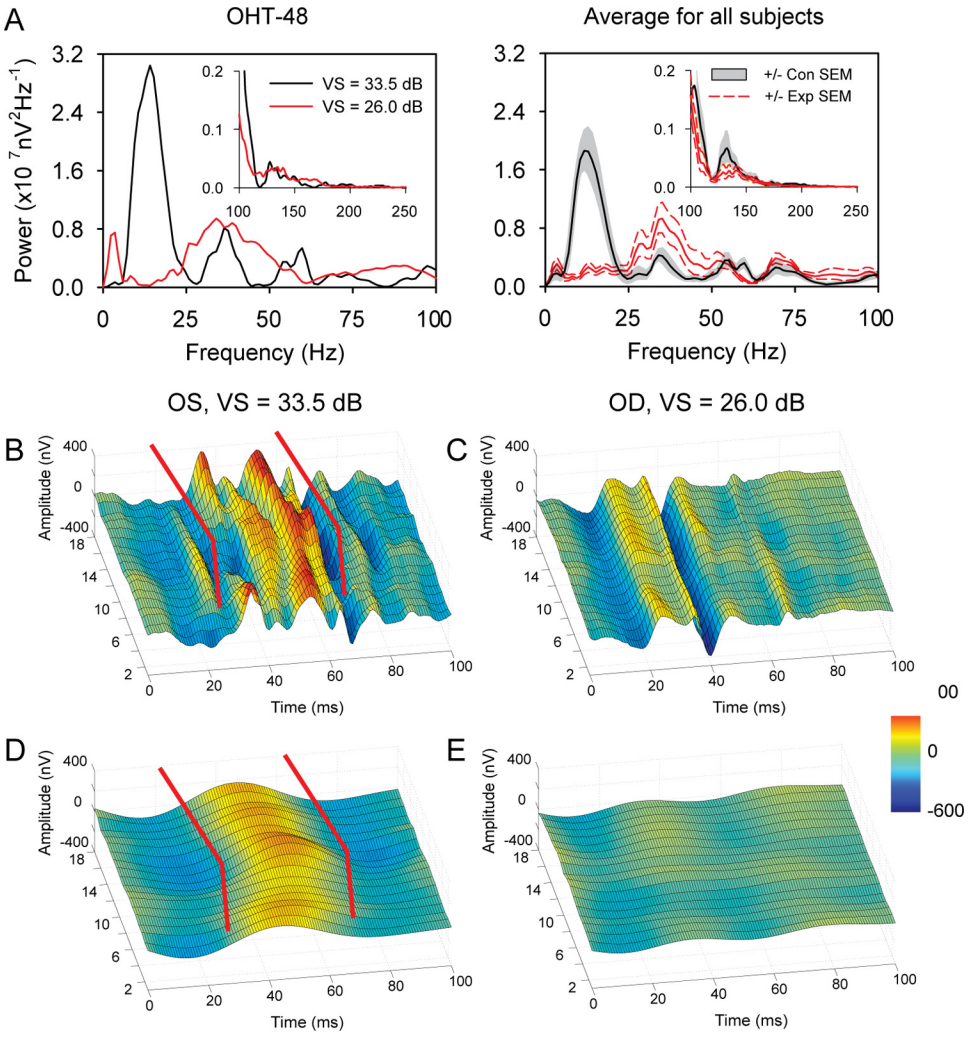

Figure 4. Effects of experimental glaucoma on mfERG signals. (**A**) *Left*: power spectra of the summed mfERG recordings from each eye of subject OHT-48; *right*: LL subjects with unilateral glaucoma. The *red lines* for Con eyes and the *gray shading* for the Exp eye indicate ±1 SEM. *Insets*: frequency range of high-frequency OPs. (**B**) 3D surface plot for the third-ring responses from the Con eye of OHT-48. (**C**) 3D surface plot for the third-ring responses from the Exp eye of OHT-48. (**D**, **E**) 3D surface plots for third-ring LFCs obtained by passing responses in (**B**) and (**C**) through a 25-Hz low-pass filter. The *red lines* in (**B**) and (**D**) are drawn parallel to the linear fits of P1 implicit time of the ONHCs (not shown).

was the average of the entire 360° of the peripapillary circular scan, PhNR amplitude was from a full-field red flash ERG, and the area covered by the 24-2 perimetry protocol is roughly twice that of the hexagon array. Therefore, there was a mismatch in area sampled for the LFC RMS amplitude compared with the other measures. To overcome these sampling problems, relations between more localized measures are presented.

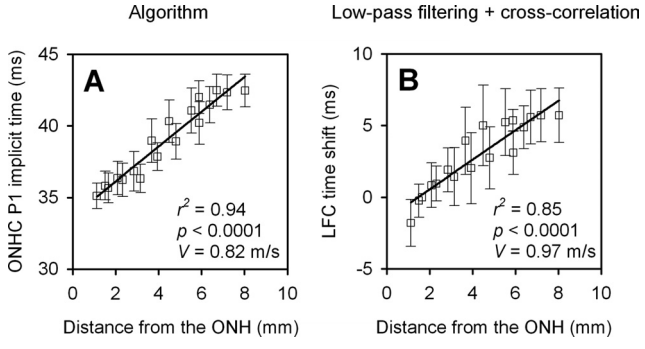

Figure 5. Axon conduction velocity estimated with two different methods (n = 7 normal eyes from seven macaques). (**A**) Axonal conduction velocity estimated from third-ring ONHC extracted with the algorithm. (**B**) Axonal conduction velocity estimated from cross-correlating third-ring LFCs. *Open squares* and error bars in both (**A**) and (**B**) represent the mean and 95% confidence interval, respectively. Velocity was calculated by dividing implicit time changes or time bin shifts by the distance from the ONH.

Relations between Regional Sectoral RNFLT and the LFC RMS for the Standard 12° OCT Peripapillary Circular Scan

The relation between local RNFLT and LFC RMS measured from hexagons could not be studied directly because of the increasing local presence, especially near the ONH, of converging axons from more remote regions of retina traveling toward the ONH. However, it was still possible to investigate the relation between RNFLT and LFC RMS for the circular scan based on the following rationale: just as the peripapillary RNFLT for each pixel of the scan is the summation of axonal input from multiple locations on the retina, the LFC RMS amplitude for each pixel should also be the summation of LFC RMS amplitudes from those locations. The structural and functional measures should co-vary for the circular scan.

The empiric axon course map of Shields[32] (Fig. 1C) was used to register hexagons with corresponding sectors on the circular scan to investigate the local relation between LFC RMS and RNFLT. In brief, projections of the hexagons on the circular scan were determined by tracing the axons along their trajectories to the ONH (Figs. 1C, 7A). LFC RMS of each hexagon was divided by the number of pixels within its pro-

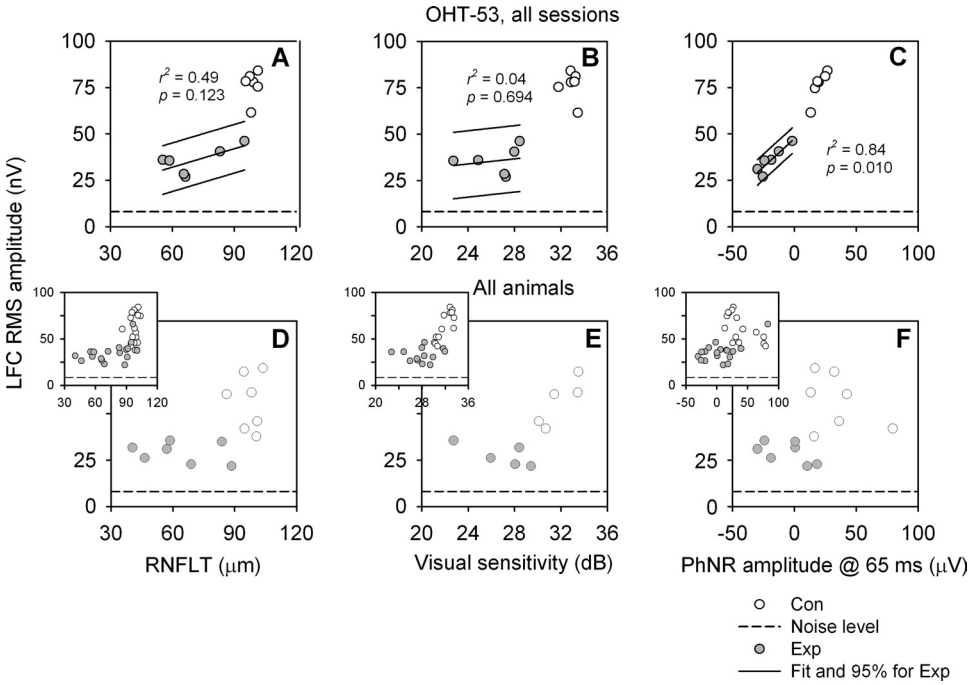

FIGURE 6. Correlation between LFC RMS amplitude of the mfERG signal averaged over the entire hexagon array and other global structure and function measures. (**A–C**) Data from all sessions for OHT-53; (**D–F**) data from the last session for each animal (*main panels*) and all sessions for all the animals (*insets*). *Solid lines*: linear fits and 95% PI for data from Exp eyes.

jection (Fig. 7A). Contributions from multiple hexagons for each pixel were summed so that an LFC RMS profile was generated. Comparisons between the circular scan and corresponding function profile were restricted to two regions on the temporal side of the disc (one superotemporal and one inferotemporal region, twelve 7° sectors altogether; Fig. 7B), which received only axon input from the central retina (the shaded area bounded by the bold axons in Fig. 1C). Relations between average sectoral RNFLT and average sectoral LFC RMS were then plotted (Figs. 7C–H), by using three different datasets. LFC RMS measures from the horizontal meridian were excluded from the integration and data analysis because of inadequate resolution to separate the dual trajectory of the axons from these hexagons to inferior and superior ONH. Data from Con and Exp eyes were considered together, as for the data in Figure 2.

Figure 7G shows the distribution of the two measures in the dataset that included all sessions from all the animals. The variability across subjects and between recording sessions created a good deal of scatter in this dataset. However, when the data from different sessions were normalized to the averages of the controls from the same examination sessions, the scatter was smaller (Fig. 7H). The slope of the fit curve to the normalized data was close to 1.

Similar effects of normalization can also be seen when only the data from the last sessions were used (Figs. 7E, 7F). Normalization improved the r^2 value from 0.44 to 0.60, and the slope of the fit curve increased from 0.19 to 1.1. The effects of normalization on data from OHT-53, however, did not improve the correlation; it changed the slope only from 0.33 to 1.2 (Figs. 7C, 7D). The effect of normalization on the slope was consistent for data from every individual animals in the study (Table 3). The fact that normalization did not improve the correlation of data from individual animals with multiple examination sessions indicated that interindividual variability was a greater contributor than intersession variability to the scatter observed in Figure 7G.

Relation between Local LFC RMS Amplitude and VS

For five of the seven animals with induced unilateral experimental glaucoma, two local functional measures, LFC RMS amplitude and interpolated VS for each hexagon, were available for comparison. Only data from the central three rings were analyzed to minimize the detrimental effects on the analysis of low SNR of RMS amplitude in more peripheral hexagons. Data from the hexagons on the horizontal meridian were again excluded from the analysis (Fig. 8A).

Figure 8B shows the inner-three-ring data from the last session for each animal in the main panel and data from all sessions of all the animals in the inset (same in Figs. 8C–E for the individual rings). Data from Con and Exp eyes followed the same trend and formed a continuous distribution (this is more obvious in the inset). In general, compared to Con eyes, the fellow Exp eyes had lower LFC RMS amplitude and VS. There was an asymptote in data distribution that was formed almost entirely by data from the Exp eyes. A single exponential curve fit both Con and Exp data distribution well ($r^2 = 0.35$; $P < 0.001$).

The noise for LFC RMS amplitude was estimated by calculating RMS amplitude for the averaged trace over the entire hexagon array in the noise window of 190 to 250 ms. The lower boundary of the 95% PI in Figure 8B approached this noise level, which was 8.2 nV on average, when VS dropped to 15 dB in glaucomatous eyes. Once LFC RMS amplitude approached its noise level, it lost capability to track further losses in VS. However, it is important to note that even with a 20-dB loss in VS, from 35 to 15 dB, 97.5% of the observed data points would still be expected to have LFC RMS amplitudes greater than the noise. The energy that was represented by this difference could be explained by the glaucoma-insensitive, low-frequency portion of the RC.

Figures 8C–E show that as eccentricity increased from the center to the periphery, LFC RMS amplitude and VS decreased in both Con and Exp eyes. Again only data from the last sessions were plotted in the main panels. The relation between LFC RMS amplitude and VS became less steep as eccentricity increased. For the most central ring, VS was not lower than 25 dB, thereby imposing no influence on formation of the asymptote. However, an increasing proportion of Exp eye data points approached the noise level as VS dropped below 25 dB with greater eccentricity, which led to reduced correlation (r^2 of the exponential fit decreased) between the two measures.

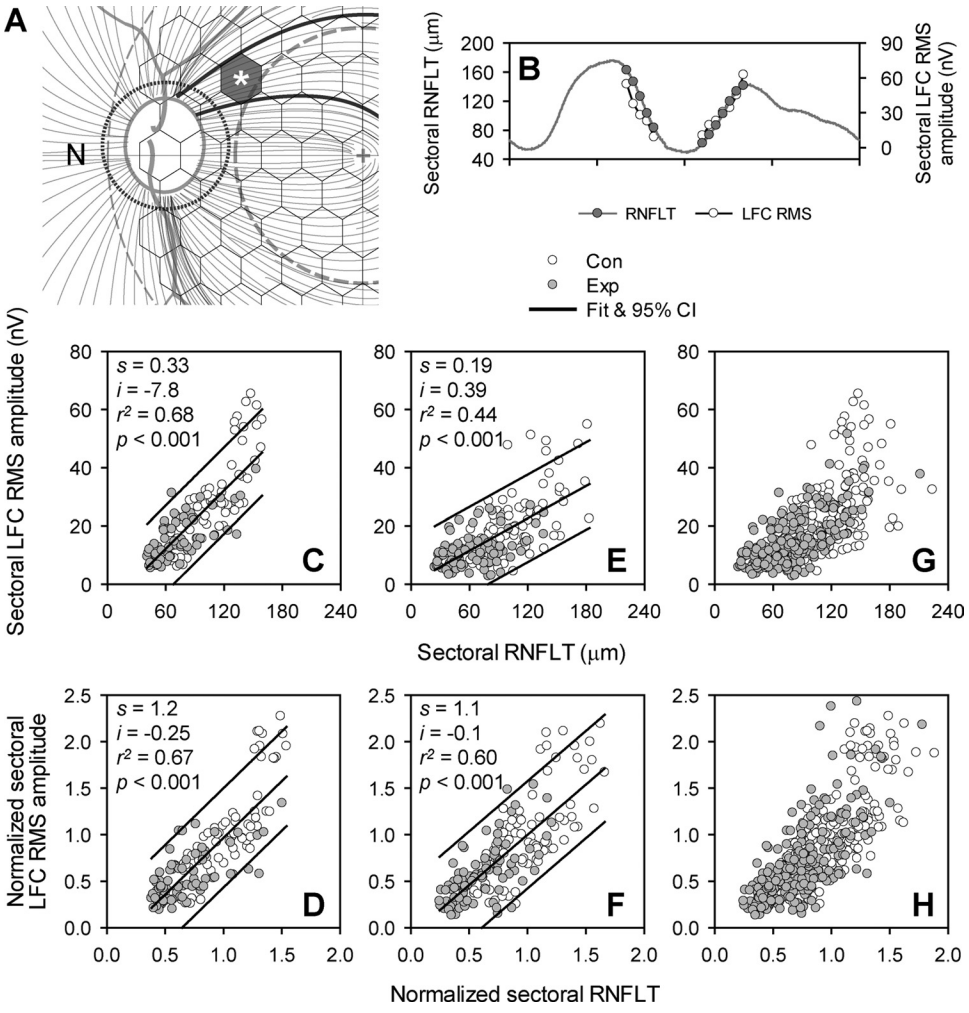

FIGURE 7. Relation between LFC RMS and peripapillary RNFLT in experimental glaucoma. (**A**) Projection of a hexagon onto a group of OCT scan pixels in the peripapillary circular scan. As described in the text, an LFC RMS "partial circular scan" was generated. Comparisons between the RNFLT and LFC RMS circular scans were restricted to two temporal regions (twelve 7° sectors) (**B**) Average sectoral RNFLT and LFC RMS amplitude profiles, both of which show changes as the location changes. (**C**) Relation between sectoral LFC RMS and RNFLT revealed with the data from all sessions for OHT-53. (**D**) Improved relation between sectoral LFC RMS and RNFLT, as data shown in (**C**) were normalized. (**E**, **F**) Relation between the LFC RMS and RNFLT before and after the data from the last session of each animal was normalized. (**G**, **H**) Distribution of LFC RMS and RNFLT measures before and after the data from all sessions for all the animals was normalized. *Solid lines*: linear fits and 95% PI for data from both Con and Exp eyes.

Table 4 lists r^2 and statistics of the exponential fits for data in Figure 8 when different datasets and animals were analyzed. The trend of weakening correlation with increasing eccentricity, seen in the group last session data, was also observed in individual last session data and particularly in the data from OHT-48, and -53, which showed more loss in VS (see Table 1) than did the other animals. Theoretically, the more profound the VS loss, the better the lower left-hand end (asymptote) of the exponential fit is defined. This contributed to the stronger correlations for OHT-48 and -53 than for the other animals.

TABLE 3. Statistics and Parameters of Linear Fits of the Relationship between RNFLT and LFC RMS Amplitude for the Temporal Side of the OCT Circular Scan

	Before Normalization				After Normalization			
Subject (*n*)	r^2	*p*	*s*	*i*	r^2	*p*	*s*	*i*
All, last session (168)	0.44	*	0.21	−1.0	0.57	*	1.14	−0.1
OHT-51 (24)	0.59	*	0.24	2.3	0.59	*	0.92	0.1
OHT-48 (24)	0.73	*	0.26	−2.0	0.73	*	1.09	−0.1
OHT-57 (48)	0.33	*	0.21	−4.4	0.33	*	1.04	−0.2
OHT-59 (72)	0.53	*	0.16	−0.7	0.52	*	1.08	0.0
OHT-60 (96)	0.43	*	0.21	−4.6	0.42	*	1.23	−0.2
OHT-61 (24)	0.78	*	0.29	−5.4	0.78	*	1.28	−0.2
OHT-53 (144)	0.68	*	0.33	−7.8	0.67	*	1.22	−0.3

The formula for the linear fit is LFC RMS amplitude = $s \cdot$ RNFLT + *i*.
* $P < 0.001$.

DISCUSSION

In the present study, we used a frequency-domain approach to identify a noninvasive electrophysiological measure that could provide an index of local function of retinal ganglion cells. The mfERG global-flash paradigm, previously shown to enhance the ONHC, was used to study local function in normal macaque eyes and eyes with experimental glaucoma. A substantial glaucoma-sensitive response in the low temporal frequency band (< 25 Hz) of the response spectrum (which we called the low-frequency component, i.e., LFC) was identified. It had nasotemporal asymmetry similar to that of ONHC, some contribution from the RC, and qualities previously attributed to the IC, and, to a lesser extent, the DC component of the mfERG. When measured globally, LFC RMS amplitude showed statistically significant correlation with PhNR amplitude. When measured locally, LFC RMS amplitude showed statistically significant correlations with corresponding peripapillary RNFLT and local VS as well.

Filter Settings for mfERG Recording

The low-frequency cutoff used for mfERG recordings was 1 Hz, which allowed us to see a large glaucoma-sensitive LFC in the global flash mfERG. Published and preliminary studies of the

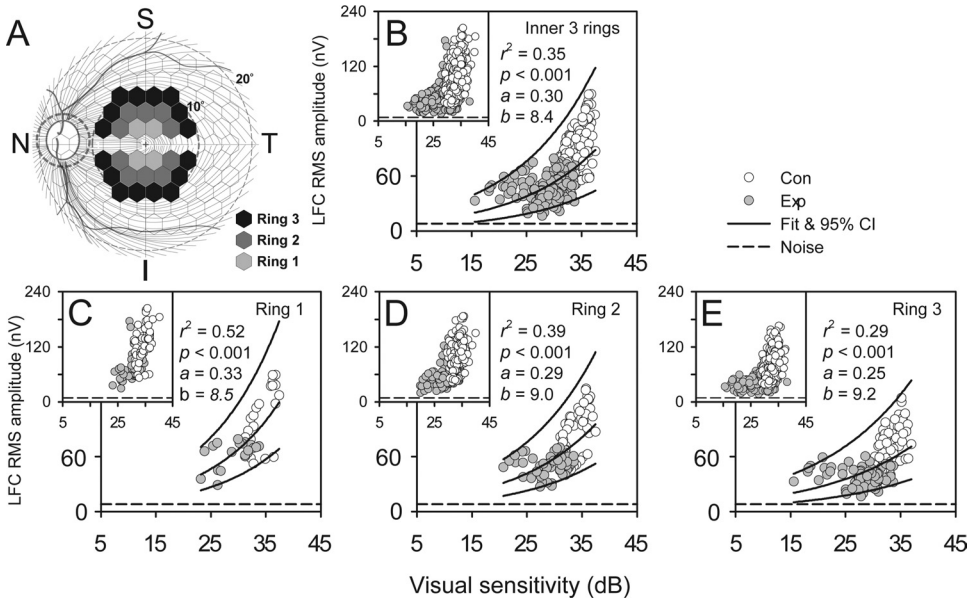

FIGURE 8. Relation between local LFC RMS amplitude and VS revealed with the data from the last experimental sessions (*main panels*) and all sessions (*insets*) of all the animals. (**A**) Data in the hexagons were from the three central rings of the global flash mfERG. (**B**) Data from all three rings and an exponential fit: LFC RMS amplitude = exp[*a*(total deviation in dB)] + *b*). (**C**–**E**) Data from the each of the three rings plotted separately. *Solid lines*: represent exponential fits and 95% PI for data from both Con and Exp eyes.

slow-sequence mfERG also show a glaucoma-sensitive LFC in macaques, obtained by filtering or manifest in multifocal (mf)PhNR, which is a low-frequency signal found in both humans and macaques[49] (Viswanathan S, et al. *IOVS* 2009;50: ARVO E-Abstract 4758; Luo X, et al. *IOVS* 2010;51:ARVO E-Abstract 1075; Kakei A, et al. *IOVS* 2010;51:ARVO E-Abstract 5473). The PhNR of the full-field and the focal flash ERG (as studied in humans and monkeys) is a glaucoma-sensitive, low-frequency response as well,[26–28,39,48,49] suggesting that the low-frequency band can provide valuable information on the functional status of glaucomatous eyes in both species. However, filter settings that are optimized for low-frequency signal, could be a problem for human subjects. The latest ISCEV guideline for clinical mfERG testing recommends that for a standard fast-flicker mfERG, the low-frequency cutoff can be any value between 3 and 10 Hz in the tradeoff with eye movement artifact.[50] The default low-frequency cutoff for the band-pass filter in the VERIS system is 10 Hz. Lowering the filter setting in the clinic to capture an LFC in the global-flash ERG is problematic for a conscious subject, since the subject must maintain good fixation while viewing the global flash stimulus, which has bright flashes that are particularly prone to eliciting eye movements. Records would be noisy and subject to frequent artifact rejection. Even for our anesthetized macaques, additional spatial averaging was needed to improve the SNR. Therefore, it may be difficult to demonstrate in humans the well-defined relationship between local RGC function and structural measures that we have observed in macaques. It also should be noted that macaques have shown more high-frequency RGC-related activity in standard fast mfERG and slow-sequence mfERG recordings than have human subjects.[41,51]

The ONHC and the LFC

The present results are consistent with a strong presence of the ONHC in the LFC of the mfERG recorded using the global-flash paradigm. However, there are several critical differences between these two glaucoma-sensitive components. The ONHC extracted with the algorithm will not, by definition, be contaminated by the RC. The LFC, however, contains the low-frequency portion of the RC and lacks a high-frequency portion of the ONHC and RC. The low-frequency portion RC probably contributed to larger 95% CIs when the LFC, rather than the extracted ONHC, was used to estimate axonal conduction velocity (Fig. 5).

In glaucomatous eyes, the low-frequency portion of the ONHC was lost, which led to loss of nasotemporal asymmetry in the LFC. As noted above, our data suggest that a small portion of the RC LFC was also affected by glaucoma. Since a- and b-wave amplitudes of white, brief, full-field flash ERG in

TABLE 4. Statistics for Exponential Fits of the Relationship between Local LFC RMS Amplitude and Visual Sensitivity

	All Three Inner Rings			Ring 1			Ring 2			Ring 3		
	n	r^2	*P*	*n*	r^2	*P*	*n*	r^2	*P*	*n*	r^2	*P*
All animals, last session	300	0.35	*	40	0.52	*	100	0.39	*	160	0.29	*
OHT-51	60	0.40	*	8	0.48	0.056	20	0.30	0.013	32	0.38	*
OHT-48	60	0.82	*	8	0.95	*	20	0.87	*	32	0.87	*
OHT-57	120	0.15	*	16	0.13	0.166	40	0.07	0.099	64	0.11	0.008
OHT-60	180	0.20	*	24	0.01	0.642	60	0.07	0.037	96	0.16	*
OHT-53	360	0.58	*	48	0.66	*	120	0.64	*	192	0.55	*

Data from the last session for each animal and for the five individual animals were fit for rings 1, 2, and 3, as well as for all three rings of hexagons in the multifocal stimulus display together.

* $P < 0.001$.

our subjects did not show significant reductions in glaucoma, consistent with the common finding in the literature, it is safe to assume that the effect on the RC in glaucomatous eyes came from the inner retina. These results suggest that an advantage of using the LFC (rather than ONHC) to monitor inner retinal function is that the LFC includes ganglion cell activity from both ONHC and RC. It is a summary index that is able to reveal loss or attenuation of the ONHC and RC and their interactions (or the DC and ICs and their interactions that occur in the time window as well). The original algorithm for ONHC extraction of Sutter and Bearse[12] required that features of the nasotemporal asymmetry be identified in the first iteration for manual alignment. As nasotemporal asymmetry deteriorates or is lost in glaucoma, it becomes increasingly more difficult to extract the ONHC reliably. Manual alignment can take time even for an experienced examiner to complete, and results may vary among examiners. One solution to this problem is to use average normative peak latency values and waveforms for RC and ONHC as templates for local RC and ONHC approximation (Bearse M, personal communication, March 2010). However, the limited number of animals available for this study precluded developing such normative data. The use of the frequency-domain approach and RMS amplitude, in contrast, provided an objective method that lead to automated and consistent measurements, for which a normative database was not required.

In a recent study, Miguel-Jimenez et al.[52] demonstrated that discrete wavelet transform (DWT) analysis could detect changes in mfERG signals recorded from patients with advanced open-angle glaucoma using the global-flash paradigm. Typical waveforms for the details of the wavelet decomposition (D_4) from normal and glaucomatous sectors look similar to the waveform changes illustrated in Figure 3B. It would be interesting to see whether glaucomatous changes identified with this method demonstrate characteristics of the ONHC, and how these functional changes identified with DWT analysis correlate with retinal structural measures.

Relation between LFC and PhNR

The correlation between LFC and PhNR was statistically significant (Fig. 6C) and roughly linear for an animal studied longitudinally. RNFLT measured with OCT has been reported to be a highly reproducible and a sensitive measure for assessing structural changes in glaucoma.[53–56] For global measures, the relation between PhNR amplitude and RNFLT (Figs. 2B, 2E) was linear, as reported previously,[57] suggesting utility for the ERG measure in assessing ganglion cell integrity. The LFC studied locally shared this characteristic. As illustrated in Figure 7, local RGC function assessed with LFC RMS amplitude, changed proportionally as sectoral RNFLT changed with experimental glaucoma when the measure was summed appropriately for the standard peripapillary circular scan and normalized to minimize variability. Both ERG measures also showed reliable changes earlier in onset of changes than VS in experimental glaucoma as previously observed.[27] Early changes in these ERG measures would be consistent with dysfunction, but not necessarily death of ganglion cells and their axons or perhaps dysfunction of glial cells whose currents contribute to the ERG. In the present study, local LFC RMS amplitudes dropped right after laser treatment and before significant VS changes were noted (Fig. 8). Table 1 shows that for two subjects (OHT-57 and -60), in early sessions LFC power losses exceeded 50%, whereas VS changes were minimal. These findings suggest that LFC, like the PhNR, may serve as a useful objective tool in detecting early RGC dysfunction.

Relations between Measures Are Determined by Their Dynamic Ranges

The relation between local RGC function assessed with mfERG LFC RMS amplitude and VS in dB was exponential (Fig. 8), which resembled the relations previously reported of RNFLT, mfVEP RMS, and global/focal PhNR with VS in patients' eyes with glaucoma and optic neuritis.[37,39,58,59] In contrast, the relation between local LFC RMS amplitude and RNFLT was roughly linear over the entire range (Fig. 7).

A fundamental determinant of the relations between these functional and structural measures is how quickly the measures being compared exhaust their dynamic ranges. VS can be quantified over a wide range, spanning four log units. LFC RMS amplitude, on the other hand, has a dynamic range of merely 100 to 200 nV, which corresponds roughly to 1 to 1.3 log units with a noise level of 8.2 nV, on average (Fig. 8), and shrinks as eccentricity increases. Dynamic ranges of RNFLT, mfVEP RMS amplitude, and PhNR amplitude measures are also limited compared with that of VS. When these measures are compared to VS, they run out of range after the first 10- to 15-dB loss of VS, creating an asymptote in the relationship as VS continues to deteriorate.

Tests with different dynamic ranges can serve different purposes. For instance, VS can follow glaucomatous change to advanced and end stages, whereas mfVEP, LFC, PhNR, and RNFLT may be of greater clinical value earlier in the disease. In clinical applications, it is also important to know how many steps of detectable change lie within the dynamic range of a particular test or how variable a particular test is.

Similarities in mfERG and mfVEP Findings with Glaucoma

The mfVEP test, when appropriately analyzed, can serve as an objective visual field to confirm or test reliability of questionable or inconsistent Humphrey visual field defects (see Ref. 60 for a review). The similarity of mfERG LFC RMS and mfVEP RMS in their asymptotic data distribution patterns suggests that the mfERG LFC is also capable of serving as an objective visual field measure (for weak to moderate changes). For macaques, more normal eyes are needed to establish the normal database from which a probability plot of LFC RMS can be established. An objective perimetry test based on this mfERG technique has potential application in animal research on glaucoma and other optic neuropathies, and clinical research as well, if it can be successfully applied to humans, which is currently under investigation.

A Limitation of Structural Measurements in the Study

In this study we used a unique method to sum up local RGC functions revealed with LFC RMS amplitude along the standard peripapillary circular scan, to correlate with the corresponding RNFLT profile. Although a statistically significant correlation between sectoral average LFC RMS amplitude and sectoral average RNFLT ($r^2 = 0.60$, $P < 0.0001$ with normalization and exponential fit) was found, predicting local retinal RGC function from RNFLT changes observed in the circular scan is still problematic because each sector receives axon input from multiple retinal locations. One way to overcome this limitation is to measure local structural changes for correlation with local functional changes. Spectral-domain OCT makes rapid scanning of a large retinal area with sufficient resolution to resolve changes in local inner retinal structures (e.g., RNFL, RGC layer, and IPL) feasible. Future studies on relations between the local RGC function revealed with mfERG and perimetry and the

structures revealed with spectral-domain OCT will help to achieve a better understanding of this critical issue.

Conclusions

In summary, similarities between LFC and ONHC of the global-flash mfERG and statistically significant correlations between regional LFC RMS amplitude, RNFLT, and VS suggest that LFC RMS amplitude of the LFC may provide a useful index for objective quantification of local RGC function and monitoring early changes caused by experimental glaucoma.

Acknowledgments

The authors thank Marcus Bearse for helpful discussions about the manuscript, Ramkumar Ramamirtham for help with ultrasound measurement of axial lengths for the animals included in this study, and Gen Miura for help with recording the ERGs.

References

1. Sutter EE, Tran D. The field topography of ERG components in man: I. The photopic luminance response. *Vision Res.* 1992;32:433–446.
2. Bearse MA Jr, Adams AJ, Han Y, et al. A multifocal electroretinogram model predicting the development of diabetic retinopathy. *Prog Retin Eye Res.* 2006;25:425–448.
3. Lai TY, Chan WM, Lai RY, Ngai JW, Li H, Lam DS. The clinical applications of multifocal electroretinography: a systematic review. *Surv Ophthalmol.* 2007;52:61–96.
4. Hood DC, Frishman LJ, Viswanathan S, Robson JG, Ahmed J. Evidence for a ganglion cell contribution to the primate electroretinogram (ERG): effects of TTX on the multifocal ERG in macaque. *Vis Neurosci.* 1999;16:411–416.
5. Hood DC, Greenstein V, Frishman L, et al. Identifying inner retinal contributions to the human multifocal ERG. *Vision Res.* 1999;39:2285–2291.
6. Frishman LJ, Saszik S, Harwerth RS, et al. Effects of experimental glaucoma in macaques on the multifocal ERG: multifocal ERG in laser-induced glaucoma. *Doc Ophthalmol.* 2000;100:231–251.
7. Hasegawa S, Takagi M, Usui T, Takada R, Abe H. Waveform changes of the first-order multifocal electroretinogram in patients with glaucoma. *Invest Ophthalmol Vis Sci.* 2000;41:1597–1603.
8. Hood DC, Greenstein VC, Holopigian K, et al. An attempt to detect glaucomatous damage to the inner retina with the multifocal ERG. *Invest Ophthalmol Vis Sci.* 2000;41:1570–1579.
9. Fortune B, Bearse MA Jr, Cioffi GA, Johnson CA. Selective loss of an oscillatory component from temporal retinal multifocal ERG responses in glaucoma. *Invest Ophthalmol Vis Sci.* 2002;43:2638–2647.
10. Fortune B, Wang L, Bui BV, Cull G, Dong J, Cioffi GA. Local ganglion cell contributions to the macaque electroretinogram revealed by experimental nerve fiber layer bundle defect. *Invest Ophthalmol Vis Sci.* 2003;44:4567–4579.
11. Rangaswamy NV, Zhou W, Harwerth RS, Frishman LJ. Effect of experimental glaucoma in primates on oscillatory potentials of the slow-sequence mfERG. *Invest Ophthalmol Vis Sci.* 2006;47:753–767.
12. Sutter EE, Bearse MA Jr. The optic nerve head component of the human ERG. *Vision Res.* 1999;39:419–436.
13. Hood DC, Bearse MA Jr, Sutter EE, Viswanathan S, Frishman LJ. The optic nerve head component of the monkey's (Macaca mulatta) multifocal electroretinogram (mERG). *Vision Res.* 2001;41:2029–2041.
14. Sutter EE, Bearse MA. The retinal topography of local and lateral gain control mechanisms. Vision Science and Its Applications. *OSA Tech Dig Ser.* 1998;1:20–23.
15. Sutter EE, Shimada Y, Li Y, Bearse MA. Mapping inner retinal function through enhancement of adaptive components in the m-ERG. Vision Science and Its Applications, *OSA Tech Dig Ser.* 1999;1:52–55.
16. Shimada Y, Li Y, Bearse MA Jr, Sutter EE, Fung W. Assessment of early retinal changes in diabetes using a new multifocal ERG protocol. *Br J Ophthalmol.* 2001;85:414–419.
17. Chu PH, Chan HH, Ng YF, et al. Porcine global flash multifocal electroretinogram: possible mechanisms for the glaucomatous changes in contrast response function. *Vision Res.* 2008;48:1726–1734.
18. Shimada Y, Bearse MA Jr, Sutter EE. Multifocal electroretinograms combined with periodic flashes: direct responses and induced components. *Graefes Arch Clin Exp Ophthalmol.* 2005;243:132–141.
19. Palmowski-Wolfe AM, Todorova MG, Orguel S, Flammer J, Brigell M. The 'two global flash' mfERG in high and normal tension primary open-angle glaucoma. *Doc Ophthalmol.* 2007;114:9–19.
20. Lung JC, Chan HH. Effects of luminance combinations on the characteristics of the global flash multifocal electroretinogram (mfERG). *Graefes Arch Clin Exp Ophthalmol.* 2010;248:1117–1125.
21. Zhou W, Rangaswamy N, Ktonas P, Frishman LJ. Oscillatory potentials of the slow-sequence multifocal ERG in primates extracted using the Matching Pursuit method. *Vision Res.* 2007;47:2021–2036.
22. Harwerth RS, Smith EL 3rd, DeSantis L. Experimental glaucoma: perimetric field defects and intraocular pressure. *J Glaucoma.* 1997;6:390–401.
23. Quigley HA, Hohman RM. Laser energy levels for trabecular meshwork damage in the primate eye. *Invest Ophthalmol Vis Sci.* 1983;24:1305–1307.
24. Harwerth RS, Vilupuru AS, Rangaswamy NV, Smith EL 3rd. The relationship between nerve fiber layer and perimetry measurements. *Invest Ophthalmol Vis Sci.* 2007;48:763–773.
25. Gotoh Y, Machida S, Tazawa Y. Selective loss of the photopic negative response in patients with optic nerve atrophy. *Arch Ophthalmol.* 2004;122:341–346.
26. Rangaswamy NV, Shirato S, Kaneko M, Digby BI, Robson JG, Frishman LJ. Effects of Spectral Characteristics of Ganzfeld Stimuli on the Photopic Negative Response (PhNR) of the ERG. *Invest Ophthalmol Vis Sci.* 2007;48:4818–4828.
27. Viswanathan S, Frishman LJ, Robson JG, Harwerth RS, Smith EL 3rd. The photopic negative response of the macaque electroretinogram: reduction by experimental glaucoma. *Invest Ophthalmol Vis Sci.* 1999;40:1124–1136.
28. Viswanathan S, Frishman LJ, Robson JG, Walters JW. The photopic negative response of the flash electroretinogram in primary open angle glaucoma. *Invest Ophthalmol Vis Sci.* 2001;42:514–522.
29. Hood DC, Frishman LJ, Robson JG, Shady S, Ahmad J, Viswanathan S. A frequency analysis of the regional variation in the contribution from action potentials to the primate multifocal ERG. Vision Science and Its Applications. *OSA Tech Dig Ser.* 1999;56–59.
30. Harwerth RS, Smith EL 3rd, DeSantis L. Behavioral perimetry in monkeys. *Invest Ophthalmol Vis Sci.* 1993;34:31–40.
31. Hood DC, Zhang X. Multifocal ERG and VEP responses and visual fields: comparing disease-related changes. *Doc Ophthalmol.* 2000;100:115–137.
32. Shields M. The optic nerve head. *Textbook of Glaucoma*. Baltimore: Williams & Wilkins; 1987:71–104.
33. Anderson DR. Ultrastructure of human and monkey lamina cribrosa and optic nerve head. *Arch Ophthalmol.* 1969;82:800–814.
34. Ogden TE. Nerve fiber layer of the macaque retina: retinotopic organization. *Invest Ophthalmol Vis Sci.* 1983;24:85–98.
35. Ogden TE. Nerve fiber layer of the primate retina: morphometric analysis. *Invest Ophthalmol Vis Sci.* 1984;25:19–29.
36. Radius RL, Anderson DR. The course of axons through the retina and optic nerve head. *Arch Ophthalmol.* 1979;97:1154–1158.
37. Hood DC. Relating retinal nerve fiber thickness to behavioral sensitivity in patients with glaucoma: application of a linear model. *J Opt Soc Am A Opt Image Sci Vis.* 2007;24:1426–1430.
38. Hood DC, Anderson SC, Wall M, Kardon RH. Structure versus function in glaucoma: an application of a linear model. *Invest Ophthalmol Vis Sci.* 2007;48:3662–3668.
39. Machida S, Toba Y, Ohtaki A, Gotoh Y, Kaneko M, Kurosaka D. Photopic negative response of focal electoretinograms in glaucomatous eyes. *Invest Ophthalmol Vis Sci.* 2008;49:5636–5644.

40. Bearse MA Jr, Shimada Y, Sutter EE. Distribution of oscillatory components in the central retina. *Doc Ophthalmol.* 2000;100: 185–205.
41. Rangaswamy NV, Hood DC, Frishman LJ. Regional variations in local contributions to the primate photopic flash ERG: revealed using the slow-sequence mfERG. *Invest Ophthalmol Vis Sci.* 2003; 44:3233–3247.
42. Fortune B, Wang L, Bui BV, Burgoyne CF, Cioffi GA. Idiopathic bilateral optic atrophy in the rhesus macaque. *Invest Ophthalmol Vis Sci.* 2005;46:3943–3956.
43. Lapuerta P, Schein SJ. A four-surface schematic eye of macaque monkey obtained by an optical method. *Vision Res.* 1995;35: 2245–2254.
44. Fukuda Y, Watanabe M, Wakakuwa K, Sawai H, Morigiwa K. Intraretinal axons of ganglion cells in the Japanese monkey (Macaca fuscata): conduction velocity and diameter distribution. *Neurosci Res.* 1988;6:53–71.
45. Gouras P. Antidromic responses of orthodromically identified ganglion cells in monkey retina. *J Physiol.* 1969;204:407–419.
46. Ogden TE, Miller RF. Studies of the optic nerve of the rhesus monkey: nerve fiber spectrum and physiological properties. *Vision Res.* 1966;6:485–506.
47. Stanford LR. Conduction velocity variations minimize conduction time differences among retinal ganglion cell axons. *Science.* 1987; 238:358–360.
48. Colotto A, Falsini B, Salgarello T, Iarossi G, Galan ME, Scullica L. Photopic negative response of the human ERG: losses associated with glaucomatous damage. *Invest Ophthalmol Vis Sci.* 2000;41: 2205–2211.
49. Kondo M, Kurimoto Y, Sakai T, et al. Recording focal macular photopic negative response (PhNR) from monkeys. *Invest Ophthalmol Vis Sci.* 2008;49:3544–3550.
50. Hood DC, Bach M, Brigell M, et al. ISCEV guidelines for clinical multifocal electroretinography (2007 edition). *Doc Ophthalmol.* 2008;116:1–11.
51. Hood DC, Frishman LJ, Saszik S, Viswanathan S. Retinal origins of the primate multifocal ERG: implications for the human response. *Invest Ophthalmol Vis Sci.* 2002;43:1673–1685.
52. Miguel-Jimenez JM, Boquete L, Ortega S, Rodriguez-Ascariz JM, Blanco R. Glaucoma detection by wavelet-based analysis of the global flash multifocal electroretinogram. *Med Eng Phys.* 2010;32: 617–622.
53. Sihota R, Sony P, Gupta V, Dada T, Singh R. Diagnostic capability of optical coherence tomography in evaluating the degree of glaucomatous retinal nerve fiber damage. *Invest Ophthalmol Vis Sci.* 2006;47:2006–2010.
54. Sihota R, Sony P, Gupta V, Dada T, Singh R. Comparing glaucomatous optic neuropathy in primary open angle and chronic primary angle closure glaucoma eyes by optical coherence tomography. *Ophthalmic Physiol Opt.* 2005;25:408–415.
55. Budenz DL, Michael A, Chang RT, McSoley J, Katz J. Sensitivity and specificity of the StratusOCT for perimetric glaucoma. *Ophthalmology.* 2005;112:3–9.
56. Budenz DL, Chang RT, Huang X, Knighton RW, Tielsch JM. Reproducibility of retinal nerve fiber thickness measurements using the stratus OCT in normal and glaucomatous eyes. *Invest Ophthalmol Vis Sci.* 2005;46:2440–2443.
57. Machida S, Gotoh Y, Toba Y, Ohtaki A, Kaneko M, Kurosaka D. Correlation between photopic negative response and retinal nerve fiber layer thickness and optic disc topography in glaucomatous eyes. *Invest Ophthalmol Vis Sci.* 2008;49:2201–2207.
58. Cheng H, Laron M, Schiffman JS, Tang RA, Frishman LJ. The relationship between visual field and retinal nerve fiber layer measurements in patients with multiple sclerosis. *Invest Ophthalmol Vis Sci.* 2007;48:5798–5805.
59. Hood DC, Greenstein VC, Odel JG, et al. Visual field defects and multifocal visual evoked potentials: evidence of a linear relationship. *Arch Ophthalmol.* 2002;120:1672–1681.
60. Hood DC, Greenstein VC. Multifocal VEP and ganglion cell damage: applications and limitations for the study of glaucoma. *Prog Retin Eye Res.* 2003;22:201–251.